KKR-ASA method in exact exchange-potential band-structure calculations

Takao Kotani*
Department of Material Physics, Osaka National Research Institute, Agency of Industrial Science and Technology, 1-8-31 Midorigaoka, Ikeda 563, Japan

Hisazumi Akai
Department of Physics, Osaka University, Toyonaka 560, Japan
(Received 13 June 1996)

We present a method of electronic band-structure calculation which incorporates the exact Kohn-Sham density-functional exchange (EXX) potential approach with the Korringa-Kohn-Rostoker (KKR) method in the atomic-sphere approximation (ASA). It takes full account of the energy dependence of the radial functions, and hence, provides more accurate treatment in principle than our previous one based on the linearized muffin-tin orbital method [Phys. Rev. Lett. **74**, 2989 (1995)]. In this method, we treat C, Si, Ge, MgO, CaO, and MnO (Antiferro-II), which were previously studied in the framework of the linear-muffin-tin orbital method with EXX. The results are basically in agreement with the old ones, though small differences produce non-negligible effects on the results. Some numerical points as well as the strict formulation of KKR in the ASA are discussed. [S0163-1829(96)09748-2]

I. INTRODUCTION

We have developed a method of band-structure calculations[1–3] in which we use the exact exchange (EXX) energy instead of the exchange energy given by the local-density approximation (LDA).[4–6] In this approach the EXX energy, which corresponds to the Fock term in the Hartree-Fock (HF) scheme, is treated as a functional of electron densities via the eigenfunctions of the Kohn-Sham (KS) equations. We define the EXX potential faithfully by following the density-functional (DF) theory, as a functional derivative of the EXX energy with respect to the electron density. The method obviously is self-interaction-free by its construction.

We have so far formulated it within the framework of the linear-muffin-tin orbital (LMTO) method in the atomic-sphere approximation (ASA). In Refs. 1 and 2, we dealt with some insulators and semiconductors, and showed that band gaps were largely enhanced from those obtained by the LDA. It was also noticed that the EXX potential had significant structures reflecting the existence of the atomic shells, as were observed in atomic calculations.[7,8] The structures are characterized by dips which correspond to the peaks of the electron radial density. The dips contribute to push down the eigenvalues of occupied states. For simple metals, on the other hand, we pointed out in Ref. 3 that the EXX method gave very similar energy-dispersion relations to those of the LDA. In that case, the dips in the EXX potentials for valence electrons are not very conspicuous, little affecting energy eigenvalues. These facts indicate that the EXX method could provide us with a common means to deal with not only rather localized states but also extended states.

In this paper, we present the EXX method combined with the Korringa-Kohn-Rostoker (KKR) band-structure calculation in the ASA. The KKR code for the LDA is based on that developed by Akai and co-workers.[9–11] As typical test cases, we choose C, Si, Ge, MgO, CaO, and MnO, which were also treated in our previous papers.[1,2] The energy dependence of the radial functions are now fully taken into account in contrast to our previous approach, where it was considered only within a linear approximation based on the ordinary LMTO-ASA with one basis function per angular momentum.[12] In this sense, the present calculations in principle should be more reliable. In addition, we need not to take care of the atomic configurations, and also are free from the so-called ghost bands, which often are encountered in the ordinary LMTO-ASA. Another advantage of the KKR-like approach is that the scheme itself provides the Green function which can be used directly for scattering theories such as impurity problems and the coherent potential approximation (CPA). It may as well serve as a single-particle Green function used in the perturbative treatment of the correlated systems.

Historically, the EXX method in the form lacking the correlation energy was first applied to atoms by Talman and Shadwick.[7] They called their method the *optimized effective potential* (OEP) method, claiming that it could be a good substitution for the HF method. Later, the OEP method was recognized as a DF method with EXX energy by Sahni, Gruenebaum, and Perdew.[13] On the other hand, Kreiger, Li, and Iafrate[14,15] developed a different type of approximation for the OEP (or EXX) potential and, very recently, it was applied to Si and Ge by Bylander and Kleinman in the framework of the pseudopotential method.[16] It was also applied to atoms[17] with a simple correlation functional which again was constructed through the KS eigenfunctions by the similar method as the EXX energy.

Our KKR-ASA results show reasonable agreements with LMTO-ASA. From practical points of view, this agreement between the two—results obtained by completely different kind of computer codes—is extremely important since the validity of the codes can be verified only through such a long way around. This is true in particular for EXX, which demands too complicated a procedure to be tested in more or less ordinary ways. As for the latter, namely, LMTO-ASA combined with EXX, we recalculate all the systems dealt

with previously,[1,2] for the following reason. As was pointed out in previous papers,[1,2] our procedure constructing the EXX potential, when combined with the ASA, gives rise to a δ-function-like contribution to the exchange potential at the atomic-sphere boundary. Though we took the contribution into account rather naively in our old calculations, it seems more natural to delete the δ function from the resulting potential. This point will be fully discussed below. The only important outcome at this stage is that this procedure reduces the band gaps of Si and other systems, giving better agreement with the calculation of Bylander and Kleinman.[16]

In Sec. II, we present our KKR-ASA-based EXX method starting from the KKR-ASA equations. In Sec. III, we present our results and discuss them in detail. In Sec. IV, we give a brief summary.

II. THEORETICAL METHOD

A. KKR-ASA

We start by reexamining the KKR-ASA equations, so that the various procedures implied by them are defined as clearly as possible. In the KKR-ASA, the space is divided into overlapping atomic spheres (AS's). The total volume of the AS's then equals the total crystal volume. Any points in the space are denoted by $(\mathbf{r},R)$, where R is the index for the AS and $\mathbf{r}=(r,\hat{\mathbf{r}})=(r,\theta,\phi)$ $(r<R)$ is the vector denoting the position in each AS. R denotes the radius of AS. We call this model space the *AS space* in the following. To construct quantum mechanics in AS space, we have to define the Hamiltonian adapted to this space. The most important points are how to construct the ∇^2 operator (kinetic-energy term) adapted to ASA, or equivalently, how to continue wave functions between AS's. This can be done by use of the free-space Green function. The *free AS-space Green function* is defined as a natural extension of an expansion of the ordinary free-space Green function $g(\mathbf{r},\mathbf{r}',E_0)=-\exp(i\sqrt{E_0}|\mathbf{r}-\mathbf{r}'|)/4\pi|\mathbf{r}-\mathbf{r}'|$. It is equally well written in different forms,

$$g(\mathbf{r},R,\mathbf{r}',R',E_0)=\delta_{RR'}g^{\mathrm{S}}(\mathbf{r},\mathbf{r}',E_0)+\sum_{L,L'} g_{RL,R'L'}(E_0)J_L(\mathbf{r})J_{L'}(\mathbf{r}'), \tag{1}$$

$$g^{\mathrm{S}}(\mathbf{r},\mathbf{r}',E_0)=-i\sqrt{E_0}\sum_L J_L(\mathbf{r}_<)H_L(\mathbf{r}_>), \tag{2}$$

where J_L (or H_L) denotes a product of the Bessel (or Hankel) functions with real spherical harmonics, i.e., $J_L(\mathbf{r},E_0)=j_l(r\sqrt{E_0})Y_{lm}(\hat{\mathbf{r}})$ [or $H_L(\mathbf{r},E_0)=h_l(r\sqrt{E_0})Y_{lm}(\hat{\mathbf{r}})$]. The above expression is valid in the case when the space is divided into nonoverlapping muffin-tin spheres and the remaining interstitial region. The extension of the above definition to the free AS-space Green function is performed simply by, first, extending the range of $\mathbf{r}$ up to $R(0\leqslant r<R)$ beyond the nonoverlapping radius. Second, as a definition, we restrict the L summation up to $l\leqslant l_{\max}$ (e.g., $l_{\max}=2$ in this paper.) Finally, the operator ∇^2_{AS} in AS space is defined through the equation

$$(-\nabla^2_{\mathrm{AS}}-E_0)g(\mathbf{r},R,\mathbf{r}',R',E_0)=\delta(\mathbf{r}-\mathbf{r}')\delta_{RR'}, \tag{3}$$

where the δ function is understood as the identity function in the functional space restricted within the above l cutoff. For the construction of the energy-independent hermite Hamiltonian from ∇^2_{AS} above, E_0 obviously cannot be dependent on the energy parameter E. In the KKR-ASA equation emerging in the standard LMTO-ASA text, we continue wave functions between AS's using the outgoing Hankel functions of energy $E_0=0$ as envelope functions.[12] Formally, such a continuation is equivalent to exploiting the present definition of ∇^2_{AS} with $E_0=0$ in the Hamiltonian. For this reason, we choose $E_0=0$ in the following though some expressions, e.g., Eq.(2), seemingly become meaningless for $E_0=0$.[18]

The total energy $E_{\mathrm{total}}[n]$ in the ASA is written as

$$E_{\mathrm{total}}[n]=E_{\mathrm{k}}[n]+E_{\mathrm{Coul}}[n_{\mathrm{s}}]+E_{\mathrm{x}}[n_{\mathrm{s}}]+E_{\mathrm{c}}[n_{\mathrm{s}}]+E_{\mathrm{ext}}[n_{\mathrm{s}}], \tag{4}$$

where $n(\mathbf{r},R)$ denotes the electron density. Note that $n_{\mathrm{s}}(r,R)=r^2\int n(\mathbf{r},R)\sin(\theta)d\theta d\phi$ denotes the spherically averaged radial density. $E_{\mathrm{k}}[n]$ is the kinetic energy of the noninteracting system as a functional of the density $n(\mathbf{r},R)$. E_{Coul}, E_{x}, E_{c}, and E_{ext} denote the Coulomb, exchange, correlation, and external potential energies as the functional of $n_{\mathrm{s}}(r,R)$, respectively. We omit spin indices for simplicity. Adding the term $\Sigma_R\int_0^R dr V_{\mathrm{eff}}(r,R)(\int r^2 n(\mathbf{r},R)\sin(\theta)d\theta d\phi - n_{\mathrm{s}}(r,R))$, with the Lagrange multiplier $V_{\mathrm{eff}}(r,R)$, we take the variation with respect to $n(\mathbf{r},R)$ and $n_{\mathrm{s}}(r,R)$ independently. We obtain the fundamental equations

$$\frac{\delta E_{\mathrm{k}}[n]}{\delta n(\mathbf{r},R)}+V_{\mathrm{eff}}(r,R)=0, \tag{5}$$

$$V_{\mathrm{eff}}(r,R)=\frac{\delta E_{\mathrm{Coul}}[n_{\mathrm{s}}]}{\delta n_{\mathrm{s}}(r,R)}+\frac{\delta E_{\mathrm{x}}[n_{\mathrm{s}}]}{\delta n_{\mathrm{s}}(r,R)}+\frac{\delta E_{\mathrm{c}}[n_{\mathrm{s}}]}{\delta n_{\mathrm{s}}(r,R)}+\frac{\delta E_{\mathrm{ext}}[n_{\mathrm{s}}]}{\delta n_{\mathrm{s}}(r,R)}, \tag{6}$$

where $V_{\mathrm{eff}}(r,R)$ is identified as the spherically symmetric one-particle effective potential. In the LDA, E_{x} is given as the explicit functional of density n_{s}. Instead, we use the exchange energy $E_{\mathrm{x}}[n_{\mathrm{s}}]$ as defined in Sec. II B. This is only the difference of our method from the ordinary LDA. For E_{c}, we use the LDA correlation energy parameterized by von Barth and Hedin.[19]

For a given spherically symmetric one-particle effective potential $V_{\mathrm{eff}}(r,R)$, we can calculate the crystal Green function $G(\mathbf{r},R,\mathbf{r}',R',E)$, from the equation $(-\nabla^2_{\mathrm{AS}}+V_{\mathrm{eff}}(r,R)-E)G(\mathbf{r},R,\mathbf{r}',R',E)=\delta(\mathbf{r}-\mathbf{r}')\delta_{RR'}$, which is equivalent to Eq. (5). It is written as

$$G(\mathbf{r},R,\mathbf{r}',R',E)=\delta_{RR'}G^{\mathrm{S}}_R(\mathbf{r},\mathbf{r}',E)+\sum_{LL'} G_{RL,R'L'}(E)\mathcal{J}_{RL}(\mathbf{r})\mathcal{J}_{R'L'}(\mathbf{r}'), \tag{7}$$

where the single-site Green function $G^{\rm S}$, single-site wave function $\mathcal{J}_{RL}$, and back scattering term (structural Green functions) $G_{RL,R'L'}$ are defined as

$$G^{\rm S}_R(\mathbf{r},\mathbf{r}',E)=g^{\rm S}(\mathbf{r},\mathbf{r}')+\int_R d^3r''g^{\rm S}(\mathbf{r},\mathbf{r}'')\times(V_{\rm eff}(r'',R)-E+E_0)G^{\rm S}_R(\mathbf{r}'',\mathbf{r}',E), \quad (8)$$

$$\mathcal{J}_{RL}(\mathbf{r},E)=J_L(\mathbf{r})+\int_R d^3r''g^{\rm S}(\mathbf{r},\mathbf{r}'')\times(V_{\rm eff}(r'',R)-E+E_0)\mathcal{J}_{RL}(\mathbf{r}'',E), \quad (9)$$

$$G_{RL,R'L'}(E)=g_{RL,R'L'}+\sum_{R''L''} g_{RL,R''L''}t_{R''L''}(E)G_{R''L'',R'L'}(E), \quad (10)$$

$$t_{RL}(E)=\int_R d^3rJ_L(\mathbf{r})(V_{\rm eff}(r,R)-E+E_0)\mathcal{J}_{RL}(\mathbf{r},E). \quad (11)$$

We will omit the E_0 index hereafter, for brevity. These equations form a complete set of equations which are needed to construct the crystal Green function $G(\mathbf{r},R,\mathbf{r}',R')$.

In actual calculations we use the following single-site quantities (I)–(V) to obtain spherical electron densities $n(r,R)$ and other quantities used for the self-consistent iteration.

(I) Regular radial wave function $\mathcal{P}_{Rl}(r,E)$:

$$\left[-\frac{d^2}{dr^2}+\frac{l(l+1)}{r^2}+V_{\rm eff}(r,R)-E\right]r\mathcal{P}_{Rl}(r,E)=0, \quad (12)$$

$$\int_0^R r^2\mathcal{P}_{Rl}(r,E)^2dr=1. \quad (13)$$

(II) Wronskians:

$$C_{Rl}(E)=\overline{R\sqrt{E_0}}W[\mathcal{P}_{Rl}(r,E),n_l(\sqrt{E_0}r)]_{\overline{R}}, \quad (14)$$

$$S_{Rl}(E)=\overline{R\sqrt{E_0}}W[\mathcal{P}_{Rl}(r,E),j_l(\sqrt{E_0}r)]_{\overline{R}}, \quad (15)$$

where the Wronskian is defined as $W[a(r),b(r)]_{r'}=r'(a(r')db(r')/dr'-b(r')da(r')/dr')$ and $W[j_l(\sqrt{E_0}r),n_l(\sqrt{E_0}r)]_r=1/(\sqrt{E_0}r)$

(III) Single-site wave function $\mathcal{J}_{RL}(\mathbf{r},E)=\mathcal{P}_{Rl}(r,E)Y_L(\hat{\mathbf{r}})/N_{Rl}(E)$: The normalization $N_{Rl}(E)$ is given by

$$N_{Rl}(E)=C_{Rl}(E)-iS_{Rl}(E). \quad (16)$$

(IV) Modified single-site Green function $\tilde{G}^{\rm S}{}_R(\mathbf{r},\mathbf{r}',E)$ (see Appendix A for definition): The imaginary parts of $\tilde{G}^{\rm S}{}_R(\mathbf{r},\mathbf{r}',E)$ coincide with $G^{\rm S}_R(\mathbf{r},\mathbf{r}',E)$ on the real axis in the complex E plane. It is written as

$$\tilde{G}^{\rm S}{}_R(\mathbf{r},\mathbf{r}',E)=\sum_L \tilde{G}^{\rm S}{}_{Rl}(E)\mathcal{P}_{Rl}(r,E)Y_L(\hat{\mathbf{r}})\mathcal{P}_{Rl}(r',E)Y_L(\hat{\mathbf{r}}'), \quad (17)$$

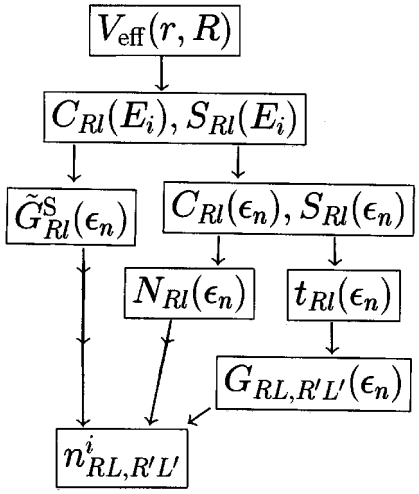

FIG. 1. Schematical veiws of the procedure calculating $n^i_{RL,R'L'}$ from $V_{\rm eff}(r,R)$.

where $\tilde{G}^{\rm S}{}_{Rl}(E)$ are analytic in the upper half-plane, and are given as functionals of $S_{Rl}(E)$ and $C_{Rl}(E)$.

(V) Atomic t matrix $t_{RL}(E)$:

$$\frac{1}{t_{RL}(E)}=-\sqrt{E_0}\left(\frac{C_{Rl}(E)}{S_{Rl}(E)}-i\right). \quad (18)$$

From these single-site quantities (I)–(V), we can construct $G(\mathbf{r},R,\mathbf{r}',R',E)$. The exchange energy $E_{\rm x}$ is calculated through $n(\mathbf{r},R,\mathbf{r}',R')$, defined by

$$n(\mathbf{r},R,\mathbf{r}',R')=-\frac{1}{\pi}{\rm Im}\int_{-\infty}^{E_{\rm F}}dEG(\mathbf{r},R,\mathbf{r}',R',E), \quad (19)$$

where we use $\tilde{G}^{\rm S}{}_R(\mathbf{r},\mathbf{r}',E)$ as a substitution for $G^{\rm S}_R(\mathbf{r},\mathbf{r}',E)$ contained in $G(\mathbf{r},R,\mathbf{r}',R',E)$. In practice, the lower bound of the integral is set at a proper energy $E_{\rm min}$ between the maximum core eigenvalue and the lowest valence eigenvalue. In all of our calculations, $E_{\rm F}-E_{\rm min}$ is chosen as 1.7∼2.0 Ry. The integration contour is deformed in the upper half-plane,[20] and the E integration mesh is written as $E=\epsilon_n$ $(n=1,\ldots,N_{\rm I})$, where the number of mesh $N_{\rm I}$ is chosen as 301. The core contribution is simply added to the integral as a discrete sum.

The single-site quantities along the complex energy contour, $C_{Rl}(E)$, $S_{Rl}(E)$, products of radial functions $\mathcal{P}_{Rl}(r,E)\mathcal{P}_{Rl}(r',E)$, and some functions needed to construct $\tilde{G}^{\rm S}{}_{Rl}(E)$ are given by the Chebyshev-expansion interpolation from the quantities $C_{Rl}(E_i)$ and $S_{Rl}(E_i)$ at the energy sampling points E_i $(i=1,\ldots,N_{\rm S})$ on the real axis. We use $N_{\rm S}=15$.

Eventually $n(\mathbf{r},R,\mathbf{r}',R')$ can be given as

$$n(\mathbf{r},R,\mathbf{r}',R')=\sum_{i=1}^{N_{\rm S}}\sum_{LL'} n^i_{RL,R'L'}\mathcal{P}_{Rl}(r,E_i)Y_L(\hat{\mathbf{r}})\times\mathcal{P}_{R'l}(r',E_i)Y_{L'}(\hat{\mathbf{r}}'), \quad (20)$$

where $n^i_{RL,R'L'}$ is calculated for a given $V_{\rm eff}(r,R)$ through a procedure shown in Fig. 1. Contributions from core electrons should be properly added in Eq. (20).

B. Exact exchange potential in the ASA

With Eq. (20), the exchange energy E_x in the ASA is written as

$$E_x = -\sum_{(RR')} W_{(RR')} \int_R \int_{R'} d^3r d^3r' \frac{n(\mathbf{r},R,\mathbf{r}',R')^2}{|\mathbf{r}+\mathbf{R}-\mathbf{r}'-\mathbf{R}'|}$$

$$= -\sum_{(RR')} W_{(RR')} \sum_{L_1L_2 i} \sum_{L_3L_4 j} n^i_{RL_1,R'L_2} n^j_{RL_3,R'L_4} I_{RR'} \times (L_1,i,L_2,i,L_3,j,L_4,j), \quad (21)$$

where (RR') denotes pairs of nonequivalent atomic sites, and $W_{(RR')}$ denotes numbers of the equivalent pairs. The quantity $I_{RR'}$ is defined as

$$I_{RR'}(L_1,i,L_2,i,L_3,j,L_4,j) = \int_R d^3r \int_{R'} d^3r' \frac{f_{RL_1 i}(\mathbf{r}) f_{R'L_2 i}(\mathbf{r}') f_{RL_3 j}(\mathbf{r}) f_{R'L_4 j}(\mathbf{r}')}{|(\mathbf{r}+\mathbf{R})-(\mathbf{r}'+\mathbf{R}')|}, \quad (22)$$

$$f_{RLi}(\mathbf{r}) = \mathcal{P}_{Rl}(r,E_i) Y_L(\hat{\mathbf{r}}). \quad (23)$$

This can be be calculated following Svane and Andersen[21,22] through the ρ and σ radial integrals in their notation. In the practical calculations shown in Sec. III, we restrict (RR') pairs up to the second-nearest pairs.

We can calculate the EXX potential $V_x(r,R) = \delta E_x / \delta n_s(r,R)$ in a similar manner to that in the LMTO-ASA case. In the DF scheme, E_x is taken as a functional of the density because it is calculated from the KS eigenfunctions, which themselves are the functionals of density through $V_{\rm eff}$. In our ASA treatment, we assume that there is a one-to-one correspondence between the spherically averaged radial density $n_s(r,R)$ and the spherically symmetric potential $V_{\rm eff}(r,R)$. Then the exchange energy E_x is given as a functional of $V_{\rm eff}(r,R)$, and hence, is also given as a functional of $n_s(r,R)$ due to the above assumption. We can calculate $V_x(r,R)$ from $\delta E_x / \delta V_{\rm eff}(r,R)$ and $\delta n(r',R') / \delta V_{\rm eff}(r,R)$. The functional derivative $\delta E_x / \delta V_{\rm eff}(r,R)$ can be calculated through Eqs. (1)–(23) using the derivative chain rule. Single-site-related parts $\delta \mathcal{P}_{Rl}(r,E_i) / \delta V_{\rm eff}(r,R)$, $\delta C_{Rl}(E_i) / \delta V_{\rm eff}(r,R)$, and $\delta S_{Rl}(E_i) / \delta V_{\rm eff}(r,R)$ are calculated through the radial Green function as was suggested by Talman and Shadwick.[7]

$\delta \widetilde{G}^{\rm S}{}_{Rl}(\epsilon_n) / \delta C_{Rl}(E_i)$ and $\delta \widetilde{G}^{\rm S}{}_{Rl}(\epsilon_n) / \delta S_{Rl}(E_i)$ are calculated numerically with the five-point differential formula. The procedure obtaining $G_{RL,R'L'}(\epsilon_n)$ from $t_{Rl}(\epsilon_n)$ is the central part of the KKR method. It imposes a matrix inversion for each k point in the Brillouin zone (BZ). For $\delta G_{RL,R'L'}(\epsilon_n) / \delta t_{Rl}(\epsilon_n)$, we use an analytic expression obtained through Eq. (10) with respect to t_{Rl}. This part is the most demanding from the computational point of view, especially when we need a large number of k points for the BZ summation. Correspondingly in our previous LMTO-ASA version, $\delta E_x / \delta$ (potential parameters) was executed numerically. $\delta n(r',R') / \delta V_{\rm eff}(r,R)$ can also be calculated in a similar manner.

Now, $V_x(r,R) = \delta E_x / \delta n_s(r,R)$ is calculated by use of the relation

$$\frac{\delta E_x}{\delta V_{\rm eff}(r,R)} = \sum_{R'} \int_0^{\overline{R}} dr' \frac{\delta n_s(r',R')}{\delta V_{\rm eff}(r,R)} \times \frac{\delta E_x[n_s]}{\delta n_s(r',R')}. \quad (24)$$

Here the summation with respect to R' is taken only within a unit cell. Note that an impuritylike potential variation is not necessary in the calculation of $\delta E_x / \delta V_{\rm eff}(r,R)$ and $\delta n_s(r',R') / \delta V_{\rm eff}(r,R)$. Instead, we take a variation $\delta V_{\rm eff}(r,R)$ for all sites simultaneously, and see the resulting density variation compatible with the crystal symmetry. In the actual procedure, the integration in Eq. (24) is replaced by the discrete sum using the trapezoidal rule for integration. Then Eq. (24) becomes a linear equation, and the EXX potential is obtained by inverting it. Our formalism can be naturally extended to the case of the full-potential KKR (FKKR) method,[23] though we have to devise some approximations for practical applications.

As discussed in Refs. 1 and 2, Eq. (24) can be solved only within an arbitrary constant when the chemical potential lies in the band gap. To eliminate this ambiguity, we may introduce a zero-temperature limit of the finite temperature DF, where $V_{\rm eff}$ is defined including the chemical potential. As an alternative, we can fix the constant by either adding or subtracting an infinitesimal number of electrons, so that the chemical potential is pinned at the band edge.[24] Fortunately, in the present case of nonmagnetic or antiferromagnetic states, such an arbitrary constant does not come into the final results. In the following sections, we equate the mean value of $V_x(r,R)$ with that of LDA's only to facilitate the comparison between the two.

Another problem we encounter in solving Eq. (24) by taking a matrix inversion is that, in general, the resulting $V_x(r,R)$'s contain a δ function in the AS. This means that we can lower the total energy by introducing some singular potentials in the AS. This is related to the fact that the boundary condition of the wave function is somehow artificial in the AS; see Sec. II for the definition of the continuity of the derivative of the wavefunctions across AS's (see also Appendix B). Though we naively took the contributions into account previously, the validity of the procedure is not so trivial. On the contrary, in the present paper we decided to neglect those singularities. This is mainly because such a singular behavior seems like an artifact due to the ASA than something of physical origin. In order to make this point clearer, we shall now look more carefully into the meaning of Eq. (24). For a trial density variation $\delta n_s(r,R) = \delta_{RR'} \delta(r-r')$, we can calculate the corresponding potential variation $\delta V_{\rm eff}(r,R)$ by taking the inversion of the matrix $\delta n_s / \delta V_{\rm eff}$. For the potential variations $\delta V_{\rm eff}(r,R)$, we then calculate $\delta E_x = \Sigma_R \int_0^{\overline{R}} dr [\delta E_x / \delta V_{\rm eff}(r,R)] \delta V_{\rm eff}(r,R)$, and we identify this as $\delta E_x / \delta n_s(r',R)$. As discussed in Appendix B, derivatives of $\delta E_x / \delta n_s(r,R)$ and $\delta n_s(r',R') / \delta V_{\rm eff}(r,R)$ with respect to r are not continuous across the AS in the sense of the ASA, despite the continuity of those in the wave functions. This is the reason why there exists a curious spike given by the δ function in $V_x(r,R)$. In order to avoid such a deficiency associated with the ASA, we suppress the local-density variation $\delta n_s(r,R) = \delta_{RR'} \delta(r-R)$ at the AS boundaries. This simply corresponds to neglecting the δ function that emerged

in the procedure solving Eq. (24). This causes unnegligible effects on the band gaps of Si, but practically nothing for alkaline metals.[3]

III. RESULTS AND DISCUSSIONS

In order to demonstrate the applicability of our method, we compare the results of various electronic structure calculations, including those obtained by the method developed in the present paper, on nonmetallic systems, for which rather strong effects of the exchange are expected. As representatives of such systems we take C, Si, Ge, MgO, CaO, and MnO. For MnO we assume the antiferro-II ordering, as was assumed in a LDA calculation.[25] We fix the lattice constants as 6.727, 10.260, 10.677, 7.942, 9.090, and 8.41 a.u. for C, Si, Ge, MgO, CaO, and MnO, respectively. Four types of schemes are used: KKR-ASA, with the exact exchange denoted as KKR EXX; LMTO-ASA, with the exact exchange denoted as LMTO EXX; KKR-ASA, with the LDA exchange denoted as KKR LDA; and LMTO-ASA, with the LDA exchange denoted as LMTO LDA.

In KKR, the Brillouin-zone summation is performed with 28 k points in the irreducible wedge of the zone, except for MnO, for which we use 19 k-points. In the LMTO, we use the same number of k points for MnO, but use 29 k points for others only for computational convenience. For C, Si, and Ge, we insert empty AS's (denoted as the E-AS's) to attain bcc packing. All AS's in each system have the same radius R except in the case of MgO. For MgO, we take 2.670 a.u. for Mg-AS and 2.215 a.u. for O-AS. These are taken from Refs. 26 and 27. The C($1s$), Si($1s2s2p$), Ge($1s2s2p3s3p$), Mg($1s2s2p$), O($1s$), Ca($1s2s2p3s$), and Mn($1s2s2p3s3p$) orbitals are treated as core states. We need to identify one principal quantum number for each l in the ordinary LMTO, but not for KKR, where all contributions from any principal quantum numbers are included. In this sense, the computational quality of the KKR-ASA corresponds to the one of the latest versions of the LMTO which uses the multiple basis for each l channel.[28] For MgO and CaO in the case of the LMTO, the O($3d$) basis is omitted from the Hamiltonian because we cannot obtain a self-consistent solution, even in the case of the LDA, when O($3d$) basis are included.[29] Considering these, we conclude that the possible sources for the differences between the results obtained by KKR and LMTO, which will be shown below, are the fact that no O($3d$) basis is used and, for CaO, no Ca($4p$) is used either, in addition to the obvious one due to the linearization employed in the LMTO. Our revised calculation presented here for the LMTO also shows some differences from our previous calculations.[1,2] They are partly due to the different treatment of the δ function appearing in the exchange potentials, as was already explained. In addition, we used different AS ratios, treated Ca($3p$) as cores for CaO,[1] and omitted the O($3d$) basis in MnO,[2] which made the difference.

Figures 2 and 3 show EXX potentials by KKR and LMTO methods. For comparison we also show the LDA exchange potential which is calculated for the electron density determined by use of the KKR EXX. The agreement between the two EXX potentials is reasonably good, though some small differences is still observed. For C, Si, and Ge, the differences increase as r comes closer to R. For CaO there is somehow a larger disagreement, which is due to the two reasons pointed out above. As discussed in previous papers, the dips in the EXX potential means that the EXX energy effectively gives some attractive forces between electrons, which makes the valence electrons more localized. At the same time it pulls down the orbital energies of the occupied states relative to that of the unoccupied ones.

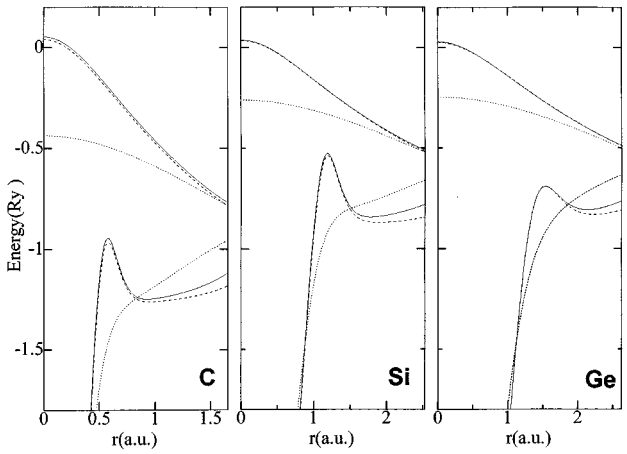

FIG. 2. Exchange potential V_x for C (diamond structure), Si, and Ge in each atomic sphere. Upper three lines are those for empty atomic-spheres (E-AS) and lower lines are for C, Si, and Ge atomic spheres (C-AS, Si-AS, and Ge-AS). The radius for C-AS of 1.656 a.u., Si-AS of 2.526 a.u., and Ge-AS of 2.629 a.u. are same as that for E-AS of each system. Solid lines are results calculated by KKR-ASA EXX and broken lines by LMTO-ASA EXX. The LDA exchange potentials denoted by dotted lines are calculated on the self-consistent density determined by KKR-ASA EXX. Each curve is shifted so that the mean value of the EXX potential agrees with that of LDA.

Table I shows the calculated total energy, the exchange energy E_x per spin, and the decomposition of E_x into core-core, core-valence, and valence-valence contribution whose classification refers to the orbital $f_{RLi}(\mathbf{r})$ appearing in Eq. (22). The valence contributions are further divided into ones from $R=R'$ and $R\neq R'$ terms. Corresponding LDA values are shown in the parentheses. Total energies calculated by the LMTO LDA are in good agreement with ones by the KKR LDA for C, Si, and Ge. The agreement is a little poorer for MgO and MnO. It is seen from those values that for C, Si, and Ge with covalent bonds, the valence contribution from $R\neq R'$ is as important as that from $R=R'$. Also seen is that for all solids the total exchange energy in KKR EXX are larger than those in LMTO EXX. The difference mainly arises in the contribution from valence $R=R'$ term. The contributions of the valence $R\neq R'$ terms to the difference are relatively small, and moreover, for MgO, CaO, and MnO, they have opposite signs to the difference in $R=R'$ contributions, partially cancelling them.

For C, Si, and Ge, the total-energy difference between KKR EXX and LMTO EXX is mostly explained by the difference in the EXX energy. The reason the band-structure calculation affects the EXX considerably may be the following: The LDA exchange energy is proportional to the $\frac{4}{3}$th power of the density, which itself is the square of the radial wave function, whereas the EXX energy contains the fourth

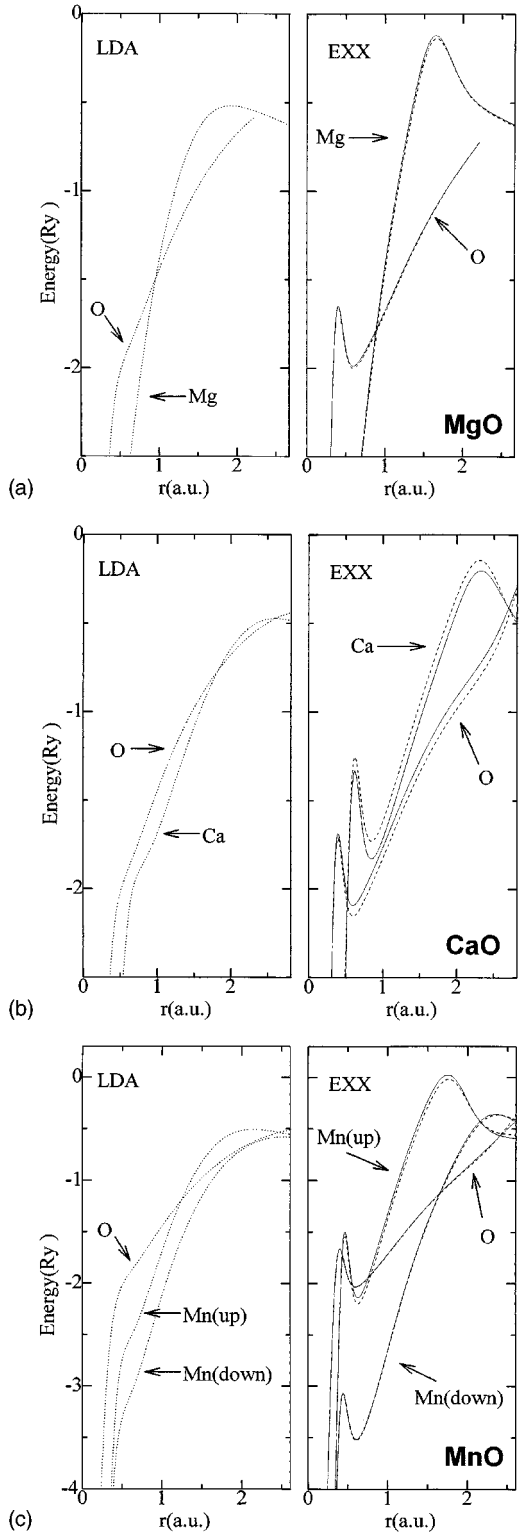

FIG. 3. Exchange potential V_x for MgO, CaO, and MnO in each atomic sphere. Solid lines are those calculated by KKR-ASA EXX, and broken lines by LMTO-ASA EXX. The LDA exchange potentials denoted by dotted lines are calculated on the self-consistent density determined by KKR-ASA EXX. Each curve is shifted so that the mean value of the EXX potential agrees with that of LDA.

power of the radial functions. The linearization approximation is hence more critical for EXX, bringing up bigger differences between KKR and LMTO cases than for corresponding LDA cases.

Table II shows the number of valence electrons per spin contained in each AS. A general tendency that the valence-band wave functions are more localized in the EXX treatment than the LDA is seen from those values. For example, the total number of electrons in each AS is enhanced for Si, Ge, and C. This means that some electrons move into the atom sites from the empty spheres. For C they are s electrons that increase. The number of p electrons in the AS is almost saturated, and cannot increase any more by localization. For Si, on the other hand, the number of p electrons increases, but that of s electrons is reduced. Such a tendency is even stronger for Ge. These things happen for the following reason. The promotion energy of forming the sp hybrids is reduced as p states become more localized. This in turn causes a larger electron transfer from s to p states. Since the energy difference between s and p states is larger for Ge than Si, the effect appears more pronounced in the former.

For the ionic systems MgO and CaO, the number of p electrons in the oxygen AS is largely increased from that of the corresponding LDA results, which simply means stronger ionicity. The situation is a little different for the transition-metal oxide MnO. In this case, both p electrons at the oxygen site and d electrons at the transition-metal site increase compared with those of the LDA results. The increase in d electrons at the transition-metal site, however, is more pronounced. This corresponds to the fact that the d states of Mn in the EXX treatment are relatively more localized than the oxygen p states. The magnetic moment of Mn is enhanced from $4.25\mu_B$ (KKR LDA) to $4.77\mu_B$ (KKR EXX). The corresponding experimental value is $4.79\mu_B$ (Ref. 30) $\sim 4.58\mu_B$.[31]

Let us now look at the results from a different, rather numerical, aspect. For a given ASA potential $V_{\rm eff}(r,R)$, there are generally some applicable methods to calculate eigenvalues. Taking the same $V_{\rm eff}(r,R)$ of Si, which is obtained by the LMTO LDA without the combined correction, as a model effective potential, we calculate the energy eigenvalues by use of the following four different methods: (a) the LMTO method without the combined correction, (b) the LMTO method with the combined correction, (c) the KKR method with $E_0=E-V_{\rm MTZ}$, and (d) the KKR method with $E_0=0$. Clearly, methods (b) and (c) cannot be categorized as an ASA as defined in Sec. II. Since $V_{\rm MTZ}$ is not given initially for the present ASA model potential, we define it as the average of $V_{\rm eff}(r,R)$ at $r=R$ weighted by the AS surface area. It is noted that the present definition of $V_{\rm MTZ}$ is considerably shallower than those used in the muffin-tin potential model. For KKR, we determine the eigenvalues by searching poles of the single-particle Green function.

The results are shown in Table III. Method (c) gives eigenvalues which are in the best agreement with the FKKR method. Comparing (a) with (b), we see that the combined correction makes the results closer to those of FKKR. The eigenvalues obtained by (d), which is used in determining the model potential, shows rather poor agreement with FKKR results, especially at $\Gamma_{2c'}$. Similar tests for CaO and MgO show that (c) again gives good agreement with non-ASA LDA calculations (see the LDA eigenvalues in Table V). This is never expected for (a) and (b) because they use minimum basis set of the LMTO.

Considering the above, we decided to calculate all eigen-

TABLE I. Exchange energy and total energy calculated by KKR-ASA EXX and LMTO-ASA EXX. Corresponding LDA values are given in the parentheses.

		Contributions to E_x per spin					
		total E_x	core	core-valence	valence $R=R'$	valence $R\neq R'$	Total energy
C	KKR	-10.380	-6.995	0.291	-1.580	-1.514	-153.379 (-151.605)
	LMTO	-10.414	-6.994	0.289	-1.614	-1.516	-153.448 (-151.608)
Si	KKR	-40.781	-38.252	0.490	-1.047	-0.992	-1160.944 (-1154.614)
	LMTO	-40.825	-38.251	0.487	-1.090	-0.996	-1161.026 (-1154.616)
Ge	KKR	-155.149	-152.384	0.815	-1.050	-0.900	-8315.201 (-8298.106)
	LMTO	-155.186	-152.394	0.809	-1.078	-0.904	-8315.290 (-8298.111)
MgO	KKR	-24.488	-20.382	0.383	-3.106	-0.617	-553.130 (-548.922)
	LMTO	-24.497	-20.384	0.379	-3.124	-0.610	-553.121 (-548.907)
CaO	KKR	-43.763	-35.321	-2.127	-6.001	-0.314	-1508.968 (-1502.396)
	LMTO	-43.764	-35.327	-2.106	-6.064	-0.268	-1508.896 (-1502.323)
MnO	KKR	-119.006	-100.883	-5.643	-11.617	-0.863	-4912.602 (-4896.799)
	LMTO	-119.012	-100.887	-5.638	-11.631	-0.856	-4912.602 (-4896.780)

TABLE II. Number of valence electron numbers for each l and spin accumulated in each AS, all calculated for EXX. Corresponding values for LDA are given in the parentheses.

		Si-AS				E-AS			
Si		s	p	d	total	s	p	d	total
KKR		0.590(0.596)	0.944(0.922)	0.094(0.088)	1.628(1.606)	0.136(0.152)	0.167(0.174)	0.069(0.069)	0.372(0.394)
LMTO		0.589(0.595)	0.949(0.922)	0.096(0.089)	1.633(1.607)	0.132(0.151)	0.164(0.173)	0.072(0.069)	0.367(0.393)
Ge		Ge-AS				E-AS			
		s	p	d	total	s	p	d	total
KKR		0.637(0.658)	0.922(0.900)	0.075(0.068)	1.634(1.626)	0.131(0.141)	0.163(0.164)	0.071(0.069)	0.366(0.374)
LMTO		0.636(0.657)	0.926(0.901)	0.077(0.069)	1.639(1.627)	0.129(0.140)	0.162(0.164)	0.071(0.069)	0.361(0.373)
C		C-AS				E-AS			
		s	p	d	total	s	p	d	total
KKR		0.498(0.485)	1.067(1.068)	0.053(0.050)	1.618(1.603)	0.147(0.158)	0.173(0.178)	0.063(0.062)	0.382(0.397)
LMTO		0.497(0.485)	1.070(1.068)	0.054(0.050)	1.620(1.603)	0.145(0.157)	0.172(0.177)	0.063(0.062)	0.380(0.397)
MgO		Mg-AS				O-AS			
		s	p	d	total	s	p	d	total
KKR		0.178(0.204)	0.313(0.341)	0.230(0.240)	0.720(0.785)	0.901(0.893)	2.372(2.314)	0.007(0.009)	3.280(3.215)
LMTO		0.175(0.201)	0.308(0.338)	0.225(0.235)	0.718(0.774)	0.901(0.892)	2.391(2.334)		3.292(3.226)
CaO		Ca-AS				O-AS			
		s	p	d	total	s	p	d	total
KKR		0.073(0.088)	3.041(3.055)	0.181(0.242)	3.295(3.385)	0.986(0.983)	2.682(2.588)	0.038(0.045)	3.705(3.615)
LMTO		0.074(0.094)	3.020(3.016)	0.178(0.269)	3.272(3.380)	0.986(0.984)	2.742(2.636)		3.728(3.620)
MnO		Mn-AS				O-AS			
		s	p	d	total	s	p	d	total
KKR	↑	0.113(0.147)	0.177(0.203)	0.190(0.467)	0.479(0.816)	0.976(0.985)	2.595(2.464)	0.064(0.108)	3.638(3.557)
	↓	0.144(0.151)	0.197(0.205)	4.911(4.713)	5.252(5.070)				
LMTO	↑	0.110(0.143)	0.173(0.199)	0.191(0.454)	0.474(0.797)	0.970(0.971)	2.600(2.477)	0.064(0.109)	3.634(3.557)
	↓	0.142(0.148)	0.196(0.203)	4.921(4.737)	5.259(5.088)				

TABLE III. Eigenvalues (in eV) for Si calculated by various different methods on the same effective potential which is determined by the LMTO-ASA LDA method without the combined correction. They are relative to the top of the valence bands.

	LMTO[a]	LMTO(CC)[b]	KKR_E[c]	KKR_0[d]	FKKR[e]
$L_{2'v}$	-9.52	-9.72	-9.54	-9.48	-9.59
L_{1v}	-6.93	-7.12	-6.95	-6.90	-6.99
$L_{3'v}$	-1.15	-1.20	-1.10	-1.13	-1.20
L_{1c}	1.64	1.41	1.43	1.61	1.48
L_{3c}	3.50	3.22	3.20	3.52	3.27
Γ_{1v}	-11.85	-12.07	-11.88	-11.83	-11.95
Γ_{15c}	2.56	2.65	2.57	2.59	2.52
$\Gamma_{2c'}$	3.93	3.08	3.27	3.88	3.34
X_{1v}	-7.73	-7.91	-7.74	-7.70	-7.79
X_{4v}	-2.75	-2.92	-2.82	-2.71	-2.87
X_{1c}	0.62	0.57	0.66	0.64	0.59
E_g	0.47	0.45	0.55	0.49	0.49

[a]LMTO-ASA without the combined correction.
[b]LMTO-ASA with the combined correction.
[c]KKR-ASA with $E_0=E-V_{\mathrm{MTZ}}$. See texts.
[d]KKR-ASA with $E_0=0$ Ry.
[e]A full-potential KKR, taken from Ref. 23.

values that are examined in the following by use of method (c), namely, the KKR method with $E_0=E-V_{\mathrm{MTZ}}$, even in the case that the self-consistent $V_{\mathrm{eff}}(r,R)$ is obtained by the LMTO method. Note that our Hamiltonian, including the operator ∇^2_{AS} defined in Eq. (3) is E dependent and not hermite any longer. This, however, is no real problem since we use the method (c) only to obtain eigenvalues for a given V_{eff}.

Eigenvalues by KKR EXX and the KKR LDA are shown in Tables IV and V and in Fig. 4 for C, Si, Ge, MgO, and CaO. Those by LMTO EXX and the LMTO LDA are also shown for comparison. In addition, in Table V, we show eigenvalues given by self-consistent muffin-tin KKR LDA calculations (denoted as KKR-T) in order to demonstrate that they are in good agreement with eigenvalues obtained by the KKR-ASA LDA.

First let us look at the difference in the eigenvalues between those obtained for the KKR and LMTO effective potentials. For the LDA potentials the eigenvalues obtained for the KKR method agree well with those by the LMTO method, except for CaO. The agreement becomes a little poorer for the EXX potentials; the KKR EXX potentials gives smaller band gaps than LMTO EXX for C, Si, and Ge, reflecting the difference in V_{x}. Now, by use of the present KKR approach, the minimum band gaps for MgO and CaO turn out 5.95 and 5.73 eV, respectively, which are significantly larger than the LDA ones, though still smaller than the respective experimental values of 7.833 and 7.09 eV. As for the band gap of Ge, we should note the following fact in order to ascertain the starting point for the comparison among various schemes. Our LDA calculation gives band gaps considerably larger than those reported in the literature. This is due to the fact that we did not perform relativistic calculations. In the LDA, a relativistic (or scalar-relativistic) treatment reduces the band gap of Ge by $\sim$0.5 eV.[32] A similar kind of shift in the eigenvalues is more or less also expected for EXX. An EXX calculation with a relativistic correction will then produce a much better agreement with experiments for the band gap of Ge. Also pointed out is that the present results have been somehow changed from the old ones[2] as a consequence of the different treatment of the δ-function contribution that was discussed in Sec. II.

Figure 5 shows eigenvalues for MnO obtained by KKR EXX, LMTO EXX, KKR LDA, and KKR-T LDA methods. The LDA minimum band gap 0.55 eV of MnO by the KKR method (0.54 eV for the LMTO) are smaller than the value 1.05 eV by the KKR-T method, where the conduction-band minimum is located in between K and U. It is therefore concluded that the discrepancy in the band gap originates from the ASA in this case. The same quantity obtained by KKR EXX is 3.38 eV, whereas it is 3.55 eV by LMTO EXX. Recent self-interaction-corrected-LDA calculations also give large band gaps of 3.57 (Ref. 33) and 3.98 eV.[34] Though, admittedly, there might be some uncertainty due to ASA both for EXX and LDA calculations, our conclusion that the EXX gives band gaps as large as the experimental one of 3.7 $\pm$0.1 (Ref. 36) could hardly be changed.

Now, let us look into the difference between EXX and the LDA in detail for the case of MnO systems. Figure 6 shows the density of states (DOS) for MnO calculated by KKR EXX and the KKR LDA, both using 189 k points. We also show the projected DOS's of Mn$\uparrow(d)$, Mn$\downarrow(d)$, and O(p). Note that the band gaps are not clearly displayed because δ functions–like the spectral function at each eigenvalue in k space—is now replaced by a Lorenzian of 0.01-Ry half-width. The magnitude of the projected DOS's of Mn$\downarrow(d)$ and O(p) for the upper edge of the highest occupied band are almost the same. The exchange splittings between $d\uparrow$ and $d\downarrow$ bands by EXX is $\approx$13 eV, which is well in agreement with the one by the SIC calculation.[33] This splitting is much larger than the LDA one of $\approx$4 eV. The DOS for MnO is different from our previous ones.[2] This discrepancy originates from the lack of an O($3d$) LMTO basis.

Clearly the biggest drawback of the present EXX approach is that we are simply using the LDA correlation. In this way we have given up a large error cancellation expected between the exchange and correlation calculated to the same order of approximations. What we can expect if we use a better correlation that balances EXX is that the effect of EXX, for example, the enhancement of the band gaps, should be largely reduced. This will make the solutions more like those of the LDA. Thus for MnO the true DF solution seems to lie somewhere in between the LDA and EXX. This expectation is rather consistent with the analysis of photoemission data,[37] where the exchange splitting of Mn(d) is $\approx$8 eV.

Now, let us turn to the system with large band gaps, namely, C, MgO, and CaO. The improvement over the LDA is again not so perfect; EXX predicts band gaps still smaller than the experimental ones by about 1–2 eV. We may point out four possible origins of the discrepancy: (i) the asphericity of V_{eff}, which is not taken into account; (ii) the correlation energy counted only by the LDA; (iii) the finite jump in

TABLE IV. Eigenvalues (in eV) calculated by KKR-ASA EXX and LMTO-ASA EXX for Si, Ge, and C (diamond). They are relative to the top of the valence bands. As for the determination of the eigenvalues, see text for further details. Corresponding values for LDA are given in the parentheses. Results obtained by muffin-tin KKR LDA are also shown.

	KKR	LMTO	Expt.[a]
Si			
$L_{2'v}$	-9.39(-9.54)	-9.33(-9.54)	
L_{1v}	-6.72(-6.95)	-6.65(-6.95)	
$L_{3'v}$	-1.05(-1.11)	-1.03(-1.10)	-1.2±0.2, -1.5
L_{1c}	1.98(1.43)	2.09(1.43)	2.1, 2.4±0.15
L_{3c}	3.50(3.20)	3.59(3.20)	4.15±0.1
Γ_{1v}	-11.69(-11.88)	-11.62(-11.88)	-12.5±0.6
Γ_{15c}	2.87(2.57)	2.95(2.57)	3.4
$\Gamma_{2'c}$	4.02(3.28)	4.15(3.27)	4.2
X_{1v}	-7.58(-7.74)	-7.52(-7.74)	
X_{4v}	-2.75(-2.82)	-2.68(-2.82)	-2.9 , -3.3±0.2
X_{1c}	1.24(0.66)	1.38(0.66)	
E_g	1.12(0.54)	1.25(0.55)	1.17
Ge			
$L_{2'v}$	-10.07(-10.37)	-10.02(-10.37)	
L_{1v}	-7.16(-7.44)	-7.11(-7.44)	-7.7±0.2, -7.4±0.2
$L_{3'v}$	-1.23(-1.30)	-1.21(-1.29)	-1.4±0.2
$L_{1c}(E_g)$	1.03(0.40)	1.12(0.40)	0.87
L_{3c}	3.79(3.64)	3.85(3.65)	4.3
Γ_{1v}	-12.20(-12.49)	-12.15(-12.50)	-12.6±0.3
$\Gamma_{2'c}$	1.57(0.60)	1.67(0.60)	0.98
Γ_{15c}	2.82(2.62)	2.88(2.62)	3.24
X_{1v}	-8.28(-8.58)	-8.23(-8.58)	
X_{4v}	-2.94(-3.03)	-2.92(-3.03)	-2.9 , -3.3±0.2
X_{1c}	1.24(0.78)	1.34(0.78)	
Diamond			
$L_{2'v}$	-15.86(-15.44)	-15.84(-15.45)	
L_{1v}	-13.28(-13.39)	-13.24(-13.39)	-12.8±0.3
$L_{3'v}$	-2.68(-2.70)	-2.67(-2.70)	
L_{3c}	8.63(8.25)	8.68(8.25)	
L_{1c}	8.97(8.97)	9.03(8.97)	
Γ_{1v}	-21.55(-21.33)	-21.52(-21.33)	-24.2±1, 21±1
Γ_{15c}	5.87(5.54)	5.92(5.53)	7.3
$\Gamma_{2'c}$	13.81(13.72)	13.89(13.73)	15.3±0.5
X_{1v}	-12.82(-12.58)	-12.80(-12.58)	
X_{4v}	-6.26(-6.30)	-6.24(-6.30)	
X_{1c}	5.24(4.75)	5.33(4.76)	
E_g	4.58(4.15)	4.65(4.16)	5.48

[a]Experimental values are taken from Ref. 40 for Si and diamond, and from Ref. 41 for Ge.

TABLE V. Eigenvalues (in eV) calculated by KKR-ASA EXX and LMTO-ASA EXX for MgO and CaO. They are relative to the top of the valence bands. As for the determination of the eigenvalues, see text for further details. Corresponding values for LDA are given in the parentheses. Results obtained by muffin-tin KKR LDA are also shown.

	KKR	LMTO	KKR-T[a]
MgO			
$L_{2'v}$	-4.10(-4.65)	-4.14(-4.69)	(-4.74)
$L_{3'v}$	-0.57(-0.71)	-0.58(-0.72)	(-0.73)
$L_{2'c}$	8.80(7.65)	8.73(7.58)	(7.56)
Γ_{1v}	-17.39(-17.02)	-17.41(-17.03)	(-17.11)
Γ_{1c}	5.95(4.60)	5.87(4.54)	(4.51)
$\Gamma_{25'c}$	17.22(15.81)	17.13(15.72)	(15.64)
$X_{4'v}$	-3.74(-4.15)	-3.77(-4.19)	(-4.23)
$X_{5'v}$	-1.19(-1.33)	-1.20(-1.34)	(-1.36)
X_{3c}	9.87(8.64)	9.79(8.56)	(8.53)
CaO			
$L_{2'v}$	-2.22(-2.74)	-2.31(-3.05)	(-2.76)
$L_{3'v}$	-0.99(-1.21)	-1.00(-1.37)	(-1.27)
$L_{2'c}$	9.15(7.01)	9.38(6.41)	(6.81)
Γ_{1c}	6.29(4.33)	6.15(3.78)	(4.47)
$\Gamma_{25'c}$	8.78(6.47)	8.97(5.51)	(6.10)
$X_{4'v}$	-1.09(-1.42)	-1.12(-1.65)	(-1.45)
$X_{5'v}$	-0.31(-0.40)	-0.32(-0.47)	(-0.41)
X_{3c}	5.73(3.46)	5.73(2.63)	(3.30)

[a]LDA calculation by the KKR method with touching muffin-tin spheres (this work).

V_x occurring at the chemical potential; and (iv) the similar jump in V_c. Concerning (i), the band gaps will be enhanced if we take account of the asphericity, because the spherical averaging smears out the large nonlinear effects arising in the exchange, reducing the energy differences between occupied and unoccupied states. On the other hand, as for (ii), using some better correlation energy beyond the LDA will reduce the band gap, as already discussed earlier in this section, since the screening effects due to the correlation obviously cancel some of the effects produced by the exchange. Since (i) and (iii) are solely related to E_x, we will be able to evaluate their effects numerically by making rather minor modifications on the present formalism (see also Ref. 24).

IV. SUMMARY

We presented a method of band calculation with the EXX energy in the framework of the KKR-ASA. The results of KKR-ASA EXX are in reasonable agreement with the results obtained by use of LMTO-ASA EXX, though there still remain some small differences that seem to come from approximations made in the LMTO. From practical points of view, the agreement of two different algorithms is very important since otherwise it was almost impossible to assert the validity of the results of such a complicated procedure as used in the EXX calculations. A minor modification of our previous results was concluded: The band gap of Si by EXX is not so large as obtained in Ref. 2, and rather close to the experimental value. Our scheme presented here will be naturally extended to the case of FKKR methods, though we have to devise some algorithms for its practical implementation.

Finally let us point out the relation between the present approach and seemingly completely different type of approaches based on the many-body perturbation theory. Among them is the GW approximation (or its extension), which is one of the most promising methods to study the electron quasiparticle spectra directly. It is reported, however, that the GW approximation starting from the LDA eigenvalues (and eigenfunctions) gives too small a band gap compared with experiments for NiO.[35] Also pointed out is that the situation is improved by imposing a self-consistency condition that the starting band gap, which is representative of the dispersion relations used for the GW approximation, should agree with the final gap obtained by this method.[35] Though the condition seems to be somewhat oversimplified, their result shows at least that the self-consistency condition is very important. Now, since such a self-consistency condition could be reformulated as the minimization principle of the Green-function functional $E[G]$ through the method of the Legendre transformation,[38] we can extend the present EXX method, which is briefly expressed by Eq. (24), to be one that can treat the above minimization problem within some tractable (maybe restricted) space of the Green function G. A study along this line is now in progress.

ACKNOWLEDGMENTS

We thank Dr. M. van Schilfgaarde, Dr. T. A. Paxton, Dr. O. Jepsen, and Dr. O. K. Andersen for the TB-LMTO program.[39] One of the authors (T.K.) acknowledges financial support due to the National Institute Post Doctoral Fellowship. Part of the present calculation has been done by use of the facilities of the Supercomputer Center, Institute for Solid State Physics, University of Tokyo.

APPENDIX A: CONSTRUCTION OF A MODIFIED SINGLE-SITE GREEN FUNCTION

We explain a method of constructing a modified single-site Green function $\tilde{G}^S{}_R(\mathbf{r},\mathbf{r}',E)$ as the substitution for the true single-site Green function $G^S_R(\mathbf{r},\mathbf{r}',E)$. The method has been exploited not only for the present calculation but also for KKR LDA calculations applied to impurity problems, the CPA, and others.[9–11] $\tilde{G}^S{}_R$ consists only of regular solutions, and is analytic in the upper half of the complex E plane. On the real axis in the E plane, the imaginary parts of the two Green functions, $\tilde{G}^S$ and G^S, are the same. In our approach, the regular and irregular solutions for the radial differential equation Eq. (13), $\mathcal{P}$ and $\mathcal{Q}$, are defined so that they satisfy

$$\mathcal{P}_l(r)=C_l(E)j_l(\sqrt{E_0}r)-S_l(E)n_l(\sqrt{E_0}r) \quad (r>\overline{R}), \tag{A1}$$

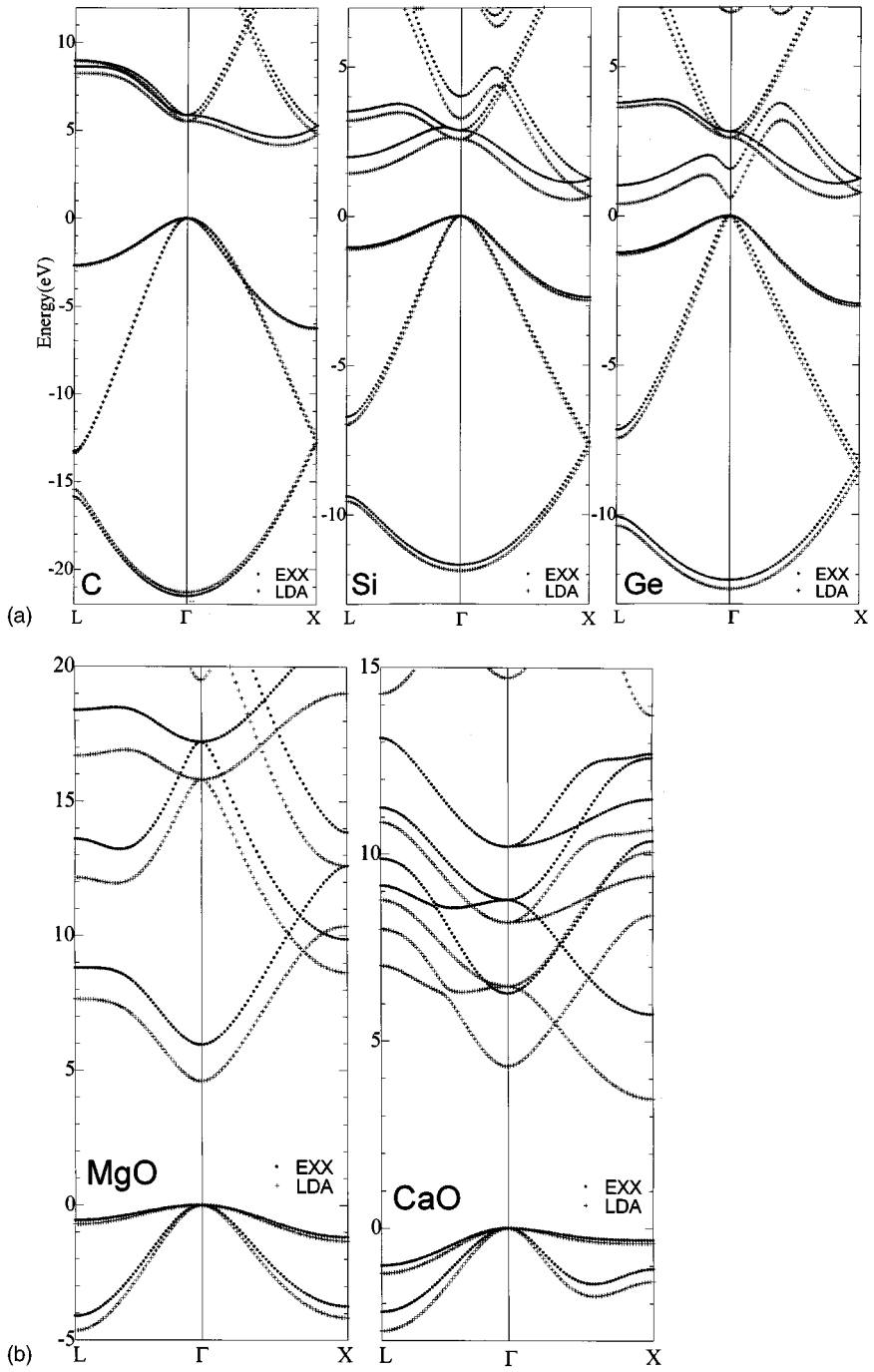

FIG. 4. Energy bands for C, Si, Ge, MgO, and CaO calculated by KKR-ASA EXX and KKR-ASA LDA. The top of the valence-band energy is set to zero. For each $V_{\rm eff}$ determined self-consistently, eigenvalues are calculated by KKR-ASA with $E_0=E-V_{\rm MTZ}$.

$$\mathcal{Q}_l(r)=S_l(E)j_l(\sqrt{E_0}r)+C_l(E)n_l(\sqrt{E_0}r) \quad (r>\overline{R}), \tag{A2}$$

where we suppress the site index R. By use of these radial solutions, $G^{\rm S}$ is expressed as the sum of each L-channel contribution, which is the product of the radial part $G_l(r,r')$ and the spherical part $Y_L(\hat{\mathbf{r}})Y_L(\hat{\mathbf{r}}')$. The radial part is

$$G_l(r,r')=\Omega_l(E)\sqrt{E_0}[\mathcal{P}_l(r_<)\mathcal{Q}_l(r_>)-i\mathcal{P}_l(r)\mathcal{P}_l(r')], \tag{A3}$$

where a normalization factor $\Omega_l(E)$ is defined as

$$\Omega_l(E)=\frac{1}{C_l(E)^2+S_l(E)^2}. \tag{A4}$$

Along the real axis, the first term of Eq. (A3) containing $\mathcal{Q}_l$ does not contribute to the charge/spin densities except for the case of core states where $\Omega_l(E)$ diverges, giving rise to an additional imaginary part to $G^{\rm S}$. The existence of the irregular solution $\mathcal{Q}_l$ causes considerable trouble in the calculation, where its expansion with respect to E is exploited. Its divergent nature can be hardly removed after such more or less interpolated treatment. Since we may treat the contribution of the core states separately, we can in principle eliminate the contribution due to $\mathcal{Q}_l$ from $G^{\rm S}$.

However, this is not true along the complex energy path. This happens because, though $G^{\rm S}$ as a whole is analytic in the upper half of the complex plane, the same is not true for each separate term of Eq. (A3). More precisely, the zeros of denominator of Eq. (A4) are exactly canceled by the zeros of

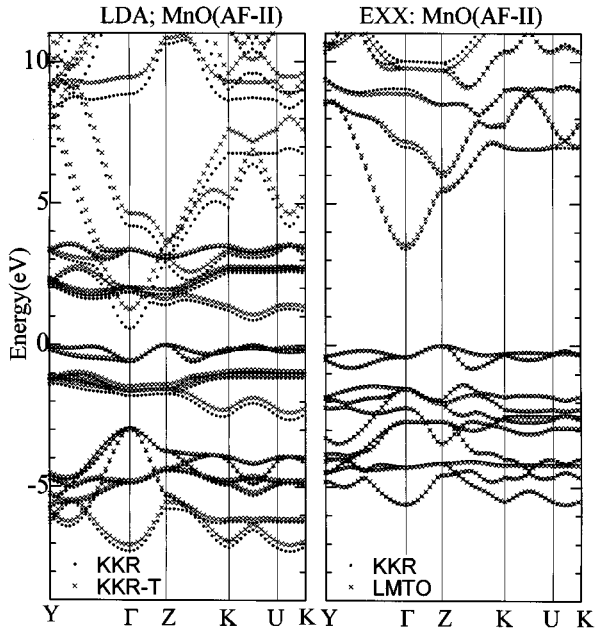

FIG. 5. Energy bands for MnO calculated by KKR-ASA EXX, LMTO-ASA EXX, and KKR-ASA LDA. For each $V_{\rm eff}$ determined self-consistently, eigenvalues are calculated by KKR-ASA with $E_0=E-V_{\rm MTZ}$. In addition, we show eigenvalues calculated by KKR with touching muffin-tin spheres (denoted by KKR-T).

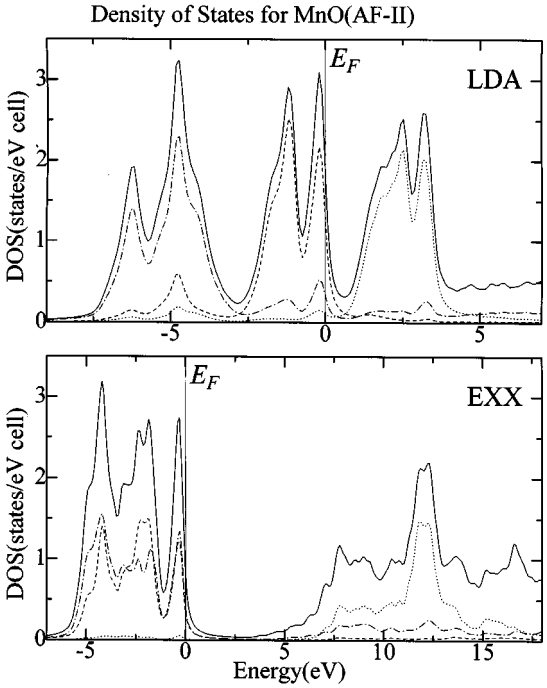

FIG. 6. Density of states for MnO calculated by KKR-ASA EXX and KKR-ASA LDA. The solid line shows the total DOS. The projected DOS is shown by the dotted line for Mn$\uparrow(d)$, the dashed line for Mn$\downarrow(d)$, and the dashed-dotted line for O(p). Note that the band gaps are not clearly shown (see the text).

$\mathcal{P}_l(r_<)\mathcal{Q}_l(r_>)+i\mathcal{P}_l(r)\mathcal{P}_l(r')$ in the upper half of the plane. In other words, residues of the poles of $\Omega_l(E)\mathcal{P}_l(r_<)\mathcal{Q}_l(r_>)$ in the upper half of the plane are canceled by $\Omega_l(E)i\mathcal{P}_l(r)\mathcal{P}_l(r')$, while ones in the lower half of the plane are just doubled.

To simulate the above exact cancellation without using $\mathcal{Q}_l$, we use the following trick. At the pole of $\Omega_l(E)$, $\mathcal{P}_l$ and $\mathcal{Q}_l$ are no longer linearly independent any more, but satisfy a relation, $\mathcal{Q}_l=[S_l(E)/C_l(E)]\mathcal{P}_l$, which can be easily verified by use of the condition $C_l(E)^2+S_l(E)^2=0$. Since the contributions from $\mathcal{Q}_l$ arise only when $C_l(E)^2+S_l(E)^2=0$ is satisfied, we may replace $\mathcal{Q}_l$ with its counterpart $[S_l(E)/C_l(E)]\mathcal{P}_l$, as a first step. This, however, brings in spurious poles due to zeros of $C_l(E)$. The second step is then to remove these singularities by introducing certain polynomials $f(E)=a_nE^n+a_{n-1}E^{n-1}+\cdots+a_0$, where $a_0,\ldots,a_n$ are real coefficients, in such a way that $\Omega_l(E)S_l(E)/C_l(E)+f(E)/C_l(E)$ does not have poles at $C_l(E)=0$. This is easily attained by fitting all $1/S_l(E_n)$'s, where E_n are the roots of $C_l(E)=0$, by a polynomial, say by the Lagrange's interpolation scheme; $f(E_n)=1/S(E_n)$ for all E_n's. Our final expression of $\widetilde{G}_l(r,r')$ is

$$\widetilde{G}_l(r,r')=\sqrt{E_0}\left[\Omega_l(E)\left(\frac{S_l(E)}{C_l(E)}-i\right)+\frac{f(E)}{C_l(E)}\right]\mathcal{P}_l(r)\mathcal{P}_l(r'). \tag{A5}$$

Now, $\widetilde{G}^{\rm S}$ is given as the sum of the $\widetilde{G}_l(r,r')Y_L(\hat{\mathbf{r}})Y_L(\hat{\mathbf{r}}')$ for all L.

APPENDIX B: δ FUNCTION ARISING IN THE EXX POTENTIAL AT THE AS BOUNDARY

We show that in the present approach δ function inevitably arises in the EXX potential at the AS boundaries. In our ASA scheme, which is characterized by $\nabla^2_{\rm AS}$ in Eq. (3), functions labeled by $(R'L')$,

$$Z_{R'L'}(\mathbf{r},R)=H_{L'}(\mathbf{r}+\mathbf{R}-\mathbf{R}',E_0), \tag{B1}$$

form a set of continuous and differentiable functions. Now, consider a function $g(\mathbf{r},R)$ which is expressed as the superposition of them. Its values at $r=R$, i.e., $f(\hat{\mathbf{r}},R)=g(R\hat{\mathbf{r}},R)$, can be written as

$$f(\hat{\mathbf{r}},R)=\sum_{R'L'}A_{R'L'}Z_{R'L'}(R\hat{\mathbf{r}},R). \tag{B2}$$

By expanding the angular dependence of this equation by spherical harmonics, we obtain an expression written as

$$f_{RL}=\sum_{R'L'}Z_{RL,R'L'}A_{R'L'}, \tag{B3}$$

where the matrix $Z_{RL,R'L'}$ is the expansion coefficient of $Z_{R'L'}(R\hat{\mathbf{r}},R)$ by spherical harmonics. In the same manner, we can obtain

$$f'_{RL}=\sum_{R'L'}Z'_{RL,R'L'}A_{R'L'}, \tag{B4}$$

where f'_{RL} denotes the expansion coefficient of the radial derivative of $g(\mathbf{r},R)$ at $r=R$. From Eqs. (B3) and (B4), we can obtain the continuity relation

$$f'_{RL}=\sum_{R'L'}(Z'\times Z^{-1})_{RL,R'L'}f_{R'L'}. \tag{B5}$$

In the framework of the ASA defined by the $\nabla^2_{\rm AS}$ in Eq. (3), any function whose values at the AS boundaries satisfy Eq. (B5) is considered continuous and differentiable at AS's. The

eigenfunctions $\psi_i(\mathbf{r},R)$'s satisfy the continuity condition Eq. (B5). On the other hand, their products generally do not satisfy such a condition.

Above in mind, let us look into the procedure determining V_x. The functional derivative of E_x with respect to the nonspherical potential $V_{\rm eff}(\mathbf{r},R)$, i.e., $\delta E_x/\delta V_{\rm eff}(\mathbf{r},R)$ can be written as

$$\frac{\delta E_x}{\delta V_{\rm eff}(\mathbf{r},R)} = -\sum_i \frac{\delta E_x}{\delta \psi_i(\mathbf{r}',R')} G(\mathbf{r}',R',\mathbf{r},R,\epsilon_i)\psi_i(\mathbf{r},R). \tag{B6}$$

Here $G(\mathbf{r}',R',\mathbf{r},R,\epsilon_i)$ satisfy the equation $[-\nabla^2_{\rm AS} + V_{\rm eff}(\mathbf{r},R)-\epsilon_i]G(\mathbf{r}',R',\mathbf{r},R,\epsilon_i)=0$ except at $(\mathbf{r},R)=(\mathbf{r}',R')$. Therefore the $(\mathbf{r},R)$ dependence of $\delta E_x/\delta V_{\rm eff}(\mathbf{r},R)$ comes from products of the eigenfunctions $G(\mathbf{r}',R',\mathbf{r},R,\epsilon_i)$ and $\psi_i(\mathbf{r},R)$. Therefore $\delta E_x/\delta V_{\rm eff}(\mathbf{r},R)$ do not satisfy Eq. (B5). The same argument follows for $\delta n(\mathbf{r}',R')/\delta V_{\rm eff}(\mathbf{r},R)$. Such is also true for their spherically averaged quantities, $\delta E_x/\delta V_{\rm eff}(r,R)$ and $\delta n_s(r')/\delta V_{\rm eff}(r,R)$. This means that neither $\delta E_x/\delta V_{\rm eff}$ nor $\delta n_s(r')/\delta V_{\rm eff}$ is continuous and differentiable at the AS. In this sense Eq. (24) does not represent a valid relation across the AS boundary. As a result the δ function appears in solving Eq. (24) with respect to $V_x(r)$. This would never happen if we exploited full-potential schemes where not only the wave functions but any physical quantities are continuous and differentiable across the cell boundary.

*Present address: Department of Physics, Osaka University, Toyonaka 560, Japan.

[1] T. Kotani, Phys. Rev. B **50**, 14 816 (1994), **51**, 13 903(E) (1995).
[2] T. Kotani, Phys. Rev. Lett. **74**, 2989 (1995).
[3] T. Kotani and H. Akai, Phys. Rev. B **52**, 17 153 (1995).
[4] R. O. Jones and O. Gunnarson, Rev. Mod. Phys. **61**, 689 (1989).
[5] R. G. Parr and W. Yang, *Density-Functional Theory of Atoms and Molecules* (Oxford University Press, New York, 1989).
[6] R. M. Dreizler and E. K. U. Gross, *Density Functional Theory* (Springer-Verlag, Berlin, 1990).
[7] J. D. Talman and W. F. Shadwick, Phys. Rev. A **14**, 36 (1976).
[8] K. Aashamar, T. M. Luke, and J. D. Talman, Phys. Rev. A **19**, 6 (1979).
[9] H. Akai, J. Phys. Condens. Matter **1**, 8045 (1989).
[10] H. Akai, M. Akai, S. Blügel, D. Dritter, H. Ebert, K. Terakura, R. Zeller, and P. H. Dedrichs, Prog. Theor. Phys. Suppl. **101**, 11 (1990).
[11] H. Akai and P. H. Dedrichs, Phys. Rev. B **47**, 8739 (1993).
[12] See, e.g., H. L. Skriver, *The LMTO Method* (Springer, New York, 1984); O. K. Andersen, O. Jepsen, and D. Glötzel, in *Highlights of Condensed-Matter Theory*, edited by F. Bassani, F. Fumi, and M. P. Tosi (North-Holland, Amsterdam, 1985), p. 59; O. K. Andersen, O. Jepsen, and M. Sob, in *Electronic Band Structure and Its Applications*, edited by M. Yussouff (Springer-Verlag, Berlin, 1986).
[13] V. Sahni, J. Gruenebaum, and J. P. Perdew, Phys. Rev. B **26**, 4371 (1982).
[14] J. B. Kreiger, Y. Li, and G. J. Iafrate, Phys. Rev. A **45**, 101 (1992).
[15] Y. Li, J. B. Kreiger, and G. J. Iafrate, Phys. Rev. A **47**, 165 (1993).
[16] D. M. Bylander and L. Kleinman, Phys. Rev. Lett. **74**, 3660 (1995); Phys. Rev. B **52**, 14 566 (1995).
[17] T. Grabo and E. K. U. Gross, Chem. Phys. Lett. **240**, 141 (1995).
[18] This actually is not the case, i.e., all the expressions are still perfectly well defined.
[19] U. von Barth and L. Hedin, J. Phys. C **5**, 1629 (1972).
[20] R. Zeller, J. Deutz, and P. H. Dedrichs, Solid State Commun. **44**, 993 (1982).
[21] A. Svane and O. K. Andersen, Phys. Rev. B **34**, 5512 (1986).
[22] A. Svane, Phys. Rev. B **35**, 5496 (1987).
[23] S. B. dear Kellen, Y. Oh, E. Badralexe, and A. J. Freeman, Phys. Rev. B **51**, 9560 (1995).
[24] In this case, the resulting $V_x(r,R)$ depends on whether we add or subtract the electron, leading to the so-called finite jump of $V_x(r,R)$. Though we can in principle calculate this jump on a basis of the present method, its numerical evaluation is a future problem.
[25] K. Terakura, T. Oguchi, A. R. Williams, and J. Kübler, Phys. Rev. B **34**, 4734 (1984).
[26] B. M. Klein, W. E. Pickett, L. L. Boyer, and R. Zeller, Phys. Rev. B **35**, 5802 (1987).
[27] When we used the AS ratio for CaO given in Ref. 26, the resulting KKR_EXX potential for Ca-AS showed an unnatural dip near $r=R$. Since the dip does not appear in the EXX LMTO potential, for which no Ca($4p$) is omitted, we conclude that an unsuitable AS ratio forced a large number of electrons to be accumulated in Ca($4p$) states. For this reason we adopt the same AS radius for Ca-AS and O-AS in the present calculation.
[28] F. Aryasetiawan and O. Gunnarson, Phys. Rev. B **49**, 7219 (1994); **49**, 16 214 (1994).
[29] We do not use the so-called downfolding prescription.
[30] B. E. F. Fender, A. J. Jacobson, and F. A. Wegwood, J. Chem. Phys. **48**, 990 (1968).
[31] A. K. Cheetham and D. A. O. Hope, Phys. Rev. B **27**, 6964 (1983).
[32] G. B. Bachelet and N. E. Christensen, Phys. Rev. B **31**, 879 (1985).
[33] Z. Szotek, W. M. Temmerman, and H. Winter, Phys. Rev. B **47**, 4029 (1993).
[34] A. Svane and O. Gunnarsson, Phys. Rev. Lett. **65**, 1148 (1990).
[35] F. Aryasetiawan and O. Gunnarson, Phys. Rev. Lett **74**, 3221 (1995).
[36] R. N. Iskenderov, I. A. Drabkin, L. T. Emel'yanova, and Ya M. Ksendzov, Fiz. Tverd. Tela (Leningrad) **10**, 2573 (1968) [Sov. Phys. Solid State **10**, 2031 (1969)].
[37] J. van Elp, R. H. Potze, H. Eskes, R. Berger, and G. A. Sawatzky, Phys. Rev. B **44**, 1530 (1991).
[38] R. Fukuda, T. Kotani, Y. Suzuki, and S. Yokojima, Prog. Theor. Phys. 92, 833 (1994).
[39] The TB-LMTO program version 4, by M. van Schilfgaarde, T. A. Paxton, O. Jepsen, and O. K. Andersen, Max-Planck-Institut für Festkörperforschung, Federal Republic of Germany (1992).
[40] M. S. Hybertsen and S. G. Louie, Phys. Rev. B **34**, 5390 (1986).
[41] M. L. Cohen and J. R. Chelikowsky, *Electric Structure and Optical Properties of Semiconductors* (Springer, New York, 1988).